Manuscript of the article: Carbon 66 (2014) 210-218.

MOLYBDENUM DOPED CARBON AEROGELS WITH CATALYTIC POTENTIAL

Balázs Nagy[1], Dániel Ábrahám[1], Gábor Dobos[2], János Madarász[3], György Onyestyák[4], György Sáfrán[5], Erik Geissler[6], Krisztina László[1*]

[1] Department of Physical Chemistry and Materials Science, Budapest University of Technology and Economics, Budapest, Hungary

[2] Department of Atomic Physics, Budapest University of Technology and Economics, Budapest, Hungary

[3] Department of Inorganic and Analytical Chemistry, Budapest University of Technology and Economics, Budapest, Hungary

[4] Institute of Materials and Environmental Chemistry, Research Centre for Natural Sciences, MTA, Budapest, Hungary

[5] Institute of Technical Physics and Materials Science, Research Centre for Natural Sciences, MTA, Budapest, Hungary

[6] Laboratoire Interdisciplinaire de Physique CNRS UMR 5588, Université J. Fourier de Grenoble, St Martin d'Hères, France.

* Corresponding author. Tel: +36-1-4631893. E-mail: klaszlo@mail.bme.hu (Krisztina László)

Abstract

Mo-doped carbon aerogels were obtained in the polycondensation reaction of aqueous resorcinol and formaldehyde by adding Mo-salt at two different stages of the synthesis: i) to the initial sol; ii) by incipient wetting impregnation of the supercritically dried polymer gel. Molybdenum added during the polymerization yielded a more compact gel structure with

practically no mesoporosity. With post-impregnation, by contrast, mesopores of diameter 3-15 nm were generated. Carbonization appreciably enhanced the microporous character of both samples, but in the mesopore range their pore size distribution was conserved. The Mo-content of the samples was also different: Mo was lost during the solvent exchange before the supercritical drying (i.e., the Mo failed to bind chemically to the polymer matrix). The residual Mo congregated into 25-60 nm bulk clusters of α-Mo_2C. In the other carbon aerogel, finely dispersed α-Mo_2C and η-Mo_3C_2 crystals formed, of size 8-20 nm. On the surface of both carbons the Mo formed oxides. In the model test reaction (acetic acid hydroconversion) the catalytic activity of both carbon aerogels was enhanced by molybdenum. The more open pore structure, higher concentration and finer Mo distribution, as well as its chemical form, may all be responsible for the greater conversion and higher value products obtained with the post-impregnated sample.

1. Introduction

Carbon aerogels that are simultaneously macro- and mesoporous offer advantages over other forms of carbons. The textural and chemical characteristics of these materials predispose them as thermal and phonic insulators, electric double layer and super capacitors, chromatography packing, adsorbents, catalyst support, etc. [1-8]. Mesoporous carbon gels can be prepared from resorcinol (R) and formaldehyde (F) under controlled conditions (solvent, concentration, stoichiometry, choice of catalyst in the precursor solution, pH, etc.) [9-11]. Most of these parameters act by influencing the mechanism and kinetics of the polycondensation process.

The tailored structure of the resorcinol-formaldehyde (RF) hydrogels can be preserved by careful removal of the solvent [12].

The selectivity and/or efficiency of these materials in catalysis or separation may be enhanced by introducing transition metals. The metal salt can, for instance, be added to the initial

resorcinol-formaldehyde solution. However, the amount of metal introduced this way is limited (typically < 1 w/w%). The synthesis of gels containing Pt [13] Ag, Mn [14] Ti [15] Cu [16] Fe, Co, Ni [17] Cr, Mo, W [18] has already been performed by this method. Enhanced incorporation of molybdate anions into RF hydrogels has recently been achieved (4-20 w/w% depending on surfactant) by adding a surfactant to the monomer solution [19].

Another method is based on the improved ion-exchange potential of the hydrogel. In this case resorcinol is substituted with 2,4-dihydroxybenzoic acid in the reaction mixture. After solvent exchange and supercritical drying the metal content in the polymer gel may reach 17 w/w%. The pore structure of the gels is conserved during the process. Fe, Ni, Co and Cu doped aerogels were prepared successfully by this method [20-23].

A third strategy is to deposit (by incipient wetness impregnation, adsorption, sublimation or supercritical deposition) the metal precursor on the dry organic, carbon or activated carbon aerogel, followed by pyrolysis or an additional heat treatment. The gels also retain their pore structure during this procedure. Pt [24], Pd [25], Ru [26] Co, Cu, Fe, Mn, Zn [27], Ni [28] and Ti [15] doped gels were prepared in this way.

During the carbonization process metal-loaded samples became partially graphitized already at around 1000 °C in the case of doping with Fe, Co, Ni, Cr [17, 29]. Reduction or even carburization of the metallic species occurs in this step to an extent that depends on the metal and the carbonization conditions [13, 18, 28, 30, 31]. The size of the metal or metal-carbide particles formed is also influenced by the carbonization conditions [13].

In this investigation resorcinol-formaldehyde (RF) aerogels and their carbonized derivatives were doped with molybdenum at different stages of the preparation. The effect of the metal on the pore size distribution and on the apparent surface area is investigated by low temperature nitrogen adsorption and high resolution transmission electron microscopy (HRTEM). Small and wide angle X-ray scattering (SAXS/WAXS), X-ray diffraction (XRD), X-ray

photoelectron spectroscopy (XPS) and selected area electron diffraction (SAED) were used to study the morphology, composition and oxidation state of the Mo-containing deposits. The catalytic potential of the molybdenum doped carbon aerogels was tested in a reductive hydrogenation reaction.

2. Experimental

2.1 Synthesis

RF polymer gels were prepared by the method of Pekala [9] modified by Lin and Ritter [10]. Resorcinol (Merck), formaldehyde (37% aq. solution, Merck) and the catalyst (C) sodium carbonate (Reanal) were dissolved in distilled water. The R/C and R/F molar ratios were 50 and 0.5, respectively, and the overall concentration of the initial solution was 5 w/w%. The pH of the system was set to 6.0. Further details are described elsewhere [12]. After water – acetone solvent exchange the wet gel was dried by supercritical carbon dioxide (scCO2) extraction [32].

Molybdenum-containing samples were prepared in two ways. i) Ammonium heptamolybdate tetrahydrate $(NH_4)_6Mo_7O_{24}.4H_2O$ (AM, Merck) was added directly to the starting reaction mixture at 0 °C. The total R/AM molar ratio and the concentration of the initial reaction mixture were 100% and 5 w/v%, respectively. The pH of the system was set again to 6.0. ii) The dry polymer aerogels were impregnated by incipient wetting (4 mL aqueous 100 g/L AM solution/ g RF aerogel). The samples were dried at 110 °C overnight. The molybdenum added to the system was identical in the two cases.

To obtain the carbon gel (CG) the dry polymer gels were carbonized in a rotary quartz reactor at 900 °C for 1 h in in a flow of high purity nitrogen (99.996%, Linde, 25 mL/min). The prehistory and the nomenclature of the samples are listed in Table 1.

Table 1. Prehistory of the samples and their symbols

Sample	Prehistory
RF	RF aerogel sample without molybdenum
MoRF	Mo-containing RF aerogel; AM salt was added to the reaction mixture
RFMo	Mo-containing RF aerogel; aqueous AM was added by incipient wetting
RF-carb	carbonized RF
MoRF-carb	carbonized MoRF
RFMo-carb	carbonized RFMo

2.2 Methods

Nitrogen adsorption/desorption isotherms were measured at -196 °C with a Nova200e (Quantachrome) computer controlled apparatus. The apparent surface area S_{BET} was calculated using the Brunauer–Emmett–Teller (BET) model [33]. The total pore volume (V_{tot}) was derived from the amount of vapour adsorbed at relative pressure 0.95, assuming that the pores are then filled with liquid adsorbate. The micropore volume (W_0) was derived from the Dubinin–Radushkevich (DR) plot [34]. The pore size distribution was calculated with the Quenched Solid State Functional Theory (QSDFT) model, assuming slit/cylindrical geometry [35]. Transformation of the primary adsorption data was performed by the Quantachrome software ASiQwin version 3.0.

The submicroscopic fine structure of the aerogels was observed by SAXS/WAXS on the BM2 small angle camera at the European Synchrotron Radiation Facility (ESRF), Grenoble, France, at 19.8 keV (0.626 Å), and also at 19.994 keV, just below the absorption edge of Mo

(19.9995 keV). The powdered samples were placed in glass capillary tubes of diameter 1.5 mm. Samples were measured in the transfer wave vector range $0.06 < q < 100$ nm^{-1}. Intensities were normalised with respect to a standard sample (lupolen).

The total molybdenum content was estimated by scanning electron microscope supported energy-dispersive X-ray spectroscopy (SEM/EDX). The investigation was carried out on a JEOL 5500 electron microscope in high vacuum mode. The samples were fastened to copper sample holders. The chemical composition of the surfaces was determined by XPS using an XR3E2 (VG Microtech) twin anode X-ray source and a Clam2 hemispherical electron energy analyzer. The base pressure of the analysis chamber was about $5 \cdot 10^{-9}$ mbar. The MgK_α radiation employed (1253.6 eV) was not monochromated. A set of mixed Gaussian-Lorentzian functions was fitted to the peaks on each spectrum after subtracting Shirley-type backgrounds using CasaXPS. Components were identified on the basis of data from reference [36]. The conventional (TEM) and high resolution transmission electron microscopy (HRTEM) investigations were carried out with Philips CM20 (200 kV) and JEOL 3010 (300 kV) electron microscopes, respectively. The morphology and structure of the samples were examined in imaging and selected area electron diffraction (SAED) modes and by fast Fourier transforms (FFT) of the HRTEM micrographs. The distribution of the elements was studied by EELS elemental mapping by means of a GATAN TRIDIEM electron energy filter. The crystallinity of the samples was examined with the same instrument in SAED (GATAN TRIDIEM) mode. XRD-ray diffraction was performed on an X'Pert Pro MPD X'Pert Pro MPD (PANalytical Bv) diffractometer in the angular range 2Θ = 4–84°, using CuK_α radiation.

2.3 Catalytic activity

The catalytic activity of the carbon aerogels was compared in the hydrogenation reaction of acetic acid (AA), a model compound for biomass [37] in a high-pressure fixed bed flow-through reactor (hydrogen pressure of 19 bar, AA pressure 2 bar) at 380 °C. The liquid fraction of the product was analyzed by a gas chromatograph (Shimadzu 2010, HP-Plot/U capillary column, flame ionization detector). The gaseous effluent was analyzed by an on-line gas chromatograph (HP 5890, Carboxen 1006 Plot capillary column, thermal conductivity detector). For all three carbon aerogels identical conditions were applied.

3. Results and discussion

3.1 Characterization of the aerogel samples

The pore structure of the aerogels was investigated by low temperature nitrogen adsorption measurements. The nitrogen adsorption/desorption isotherms and the pore size distribution (PSD) curves are shown in Figures 1 and 2, respectively. The porosity data deduced from the isotherms are listed in Table 2.

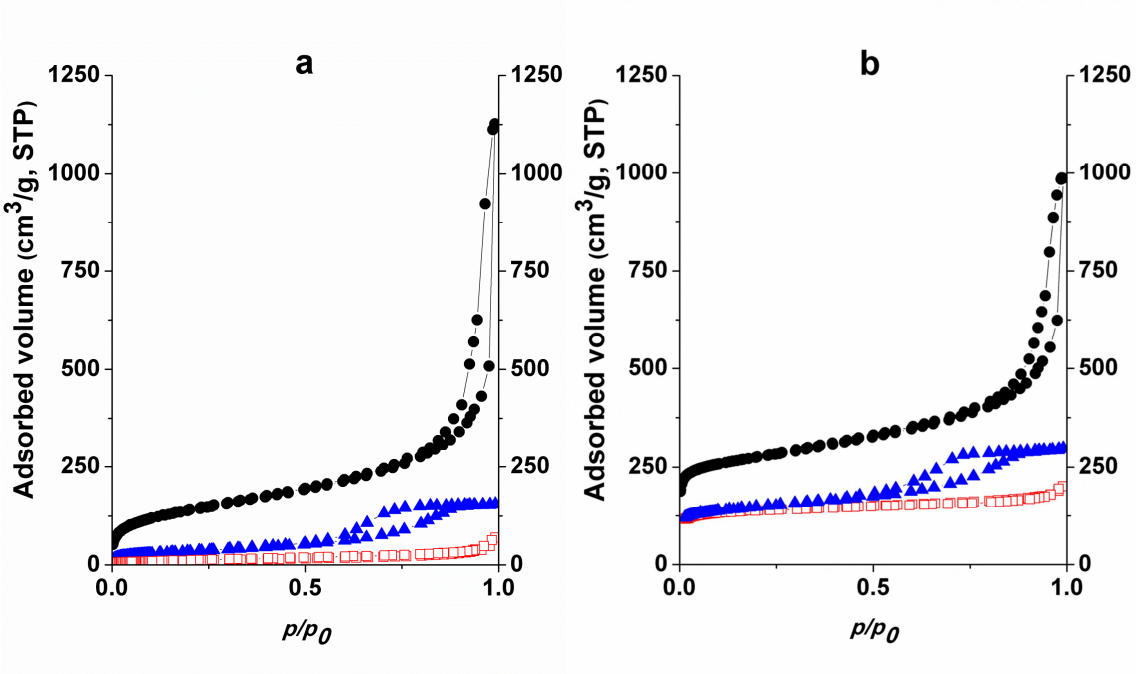

Figure 1 Low temperature nitrogen isotherms of polymer (a) and carbon (b) aerogels.

● RF (a) and RF-carb (b), □ MoRF (a) and MoRF-carb (b),

▲ RFMo (a) and RFMo-carb (b)

Table 2. Data reduced from low temperature nitrogen adsorption and SAXS measurements*

	S_{BET}	W_0	V_{tot}	$V_{0.95}$	V_{meso}	V_{macro}	R
	m^2/g	cm^3/g	cm^3/g	cm^3/g	cm^3/g	cm^3/g	nm
RF	483	0.179	1.743	0.668	0.489	1.075	7.3 [a]
MoRF	40	0.014	0.092	0.058	0.044	0.034	24.6 [b]
RFMo	124	0.046	0.239	0.236	0.190	0.003	8.0 [a]
RF-carb	1015	0.420	1.530	0.860	0.440	0.670	6.0 [a]
MoRF-carb	521	0.210	0.310	0.272	0.062	0.038	13.8 [b]
RFMo-carb	544	0.210	0.445	0.440	0.230	0.005	6.1 [a]

* S_{BET}: specific surface area from BET model, W_0: micropore volume from DR method, V_{TOT}: pore volume at $p/p_0 \rightarrow 1$, $V_{0.95}$: pore volume at $p/p_0 = 0.95$, V_{meso}: $V_{0.95}$-V_{micro}; V_{macro}: V_{TOT}-$V_{0.95}$. R: radius of the spherical elementary beads from SAXS measurements: [a]from $I(q)q^4$ vs q; [b]from extrapolation using eq 3

The shape of the isotherms indicates that the pore structure of the gels is strongly influenced by the synthesis route. The adsorption isotherms of both Mo-free aerogels show that these samples have the highest nitrogen adsorption capacity in the whole relative pressure range. Significant macroporosity with a size just beyond the detection range of the nitrogen adsorption technique develops in these samples. The molybdenum salt present during the gelation process substantially obstructs the porosity [38]. The apparent surface area of the MoRF sample is very low and no mesoporosity is detected. Incipient impregnation results in a modest reduction both in the size and volume of the mesopores of the polymer aerogel. In the

carbonized samples the dramatic change in the apparent surface area is the sign that microporosity has developed. The heat treatment also leads to an enhancement of the nitrogen adsorption in the initial section of the isotherms. Otherwise the PSD of all the three samples is conserved during the heat treatment [12].

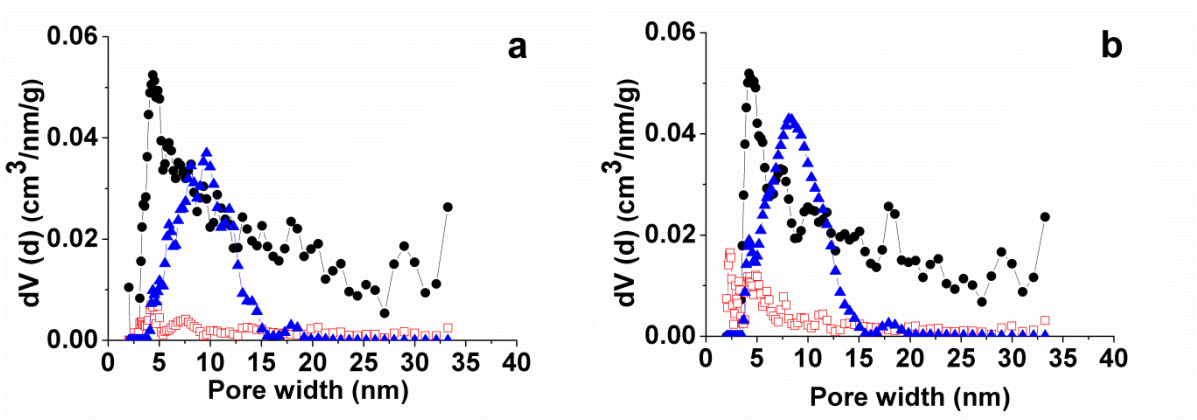

Figure 2 Mesopore size distribution (QSDFT, slit/cylindrical geometry) of the dry polymer (a) and carbon (b) aerogels. ● RF (a) and RF-carb (b), □ MoRF (a) and MoRF-carb (b), ▲ RFMo (a) and RFMo-carb (b)

3.2 SAXS results

Figure 3a shows the SAXS responses of samples RF, RFMo and RFMo-carb. Figure 3b shows those of MoRF and MoRF-carb. In Figure 3a the responses all have a similar appearance in the SAXS region. Significant differences become visible only in the WAXS region $q \geq 10$ nm^{1}, revealing the crystallinity of the molybdenum compounds. The inset in this figure is an example of the oscillations that appear at low q in a plot of $I(q)q^4$ vs q, which are the signature of the basic bead-like structure of these aerogels. The outer radius R of the beads is found by assimilating the beads to solid spheres. In the $I(q)q^4$ representation the first maximum of the scattering intensity occurs when

$$R=2.74/q_{max}\,, \qquad (1)$$

where q_{max} is the position of the maximum.

For the gels synthesized with Mo (Figure 3b), the structure differs substantially from those without: in the observed low q range, only power law behaviour is visible, of the form

$$I(q) = Aq^{-m} \quad (2)$$

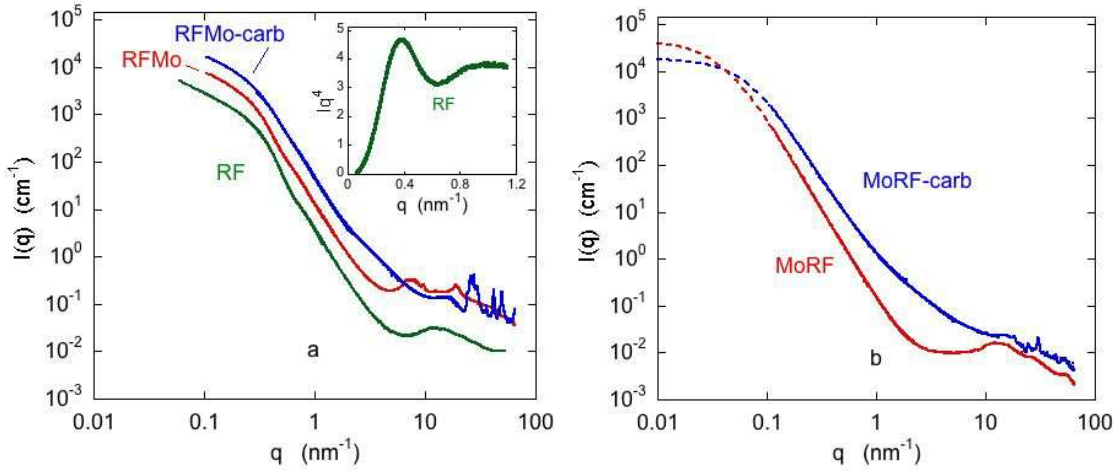

Figure 3 SAXS response of the different aerogels at 19.8 keV, a) aerogels prepared without Mo in the precursor mixture. Inset: the maximum in the plot of $I(q)q^4$ at q_{max} is characteristic of a bead-like structure with radius R=2.74/q_{max}=7.3 nm; b) aerogels prepared with Mo in the precursor mixture. The dashed extrapolations are fits to eq 3.

where the slopes m are slightly less than 4. This is surface scattering. Since no evidence of a shoulder is apparent, the elementary clusters are significantly larger than those in Figure 3a. The slope of the power law, however, enables an extrapolation to be made to lower q by using the Debye-Bueche expression [39]

$$I(q) = a/[1+(Rq)^2]^2 \quad (3)$$

The resulting extrapolations are shown as dashed lines in Figure 3b. The corresponding values of R (Table 2) suggest that carbonization of MoRF to MoRF-carb shrinks the radius of the clusters appreciably (from 24.6 to 13.8 nm).

Inspection of Table 2 shows that similar shrinkage in the bead size also occurs when the gels synthesized without Mo are carbonized. It can also be seen that the incipient impregnation has

little influence on the bead size. When Mo is present during the polymerisation, however, the low q feature moves to lower q (Figure 3b), i.e., the Mo catalyst favours much larger clusters in the aerogel.

When the incident energy of the X-ray beam is raised to 19.994 keV, just below the atomic absorption threshold of Mo (19.9995 keV), the effective number of electrons in the Mo atom decreases, and anomalous scattering effects appear. The difference in intensity between the measurements at high (E_2) and low energy (E_1) is then

$$\Delta I(q)=I_{19.8\ \mathrm{keV}}(q)-I_{19.994\mathrm{keV}}(q)$$

$$= r_0^2[\rho_{Mo}(E_1)- \rho_{Mo}(E_2)]\{2\rho_p\, S_{Mop}(q) + [\rho_{Mo}(E_1)+\rho_{Mo}(E_2)]\, S_{MoMo}(q)\} \qquad (4)$$

where r_0 is the classical radius of the electron, ρ_p and ρ_{Mo} are respectively the electron densities of the RF polymer and of the molybdenum, and $S_{Mop}(q)$ and $S_{MoMo}(q)$ are respectively the cross and direct partial structure factors of the polymer and molybdenum. $\Delta I(q)$ is thus essentially proportional to the difference in electron density of the molybdenum at the two energies, and to the amount of Mo present. As the electron density of Mo is significantly higher than that of the polymer, ρ_p, the second (direct) term in the curly brackets dominates.

Figure 4 shows the scattering intensity of sample RFMo at the two energies 19.8 and 19.994 keV, and their difference. The shape of $\Delta I(q)$ closely resembles that of $I_{19.8\ \mathrm{keV}}(q)$, and in the representation $\Delta I(q)q^4$ vs q it displays a peak at q=0.375 nm^{-1}(inset). The intensity of $\Delta I(q)$ is one order of magnitude smaller than $I(q)$, which is consistent with the difference in the number of electrons in the Mo atom participating in the scattering at these two energies, $n_{19.800\mathrm{keV}} - n_{19.994\mathrm{keV}}$ = 3.67 e [40], i.e. about 10% of the available electrons in the Mo atom. These results indicate that the principal contribution to the SAXS intensity from this sample comes from molybdenum-rich beads of approximate radius 7.3 nm. The power law slope of -4 in the region q>0.3 nm^{-1} testifies that the surface of the beads is smooth.

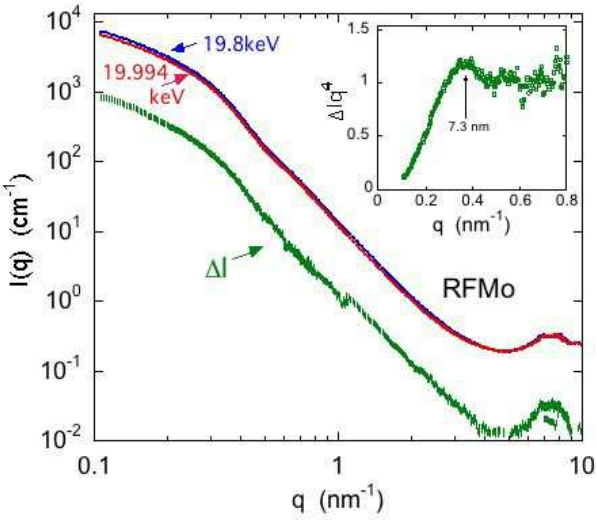

Figure 4. SAXS response from the polymer RFMo at 19.8 keV (blue symbols) and 19.994 keV (red symbols), and the difference signal $\Delta I(q)$ (green). Inset shows the maximum of $\Delta I(q)q^4$ at 0.375 nm^{-1}, corresponding to R=7.3 nm. (On the scale of this figure the responses at the two energies are so close that their symbols almost appear as a single colour. Only their difference $\Delta I(q)$ is distinguishable.)

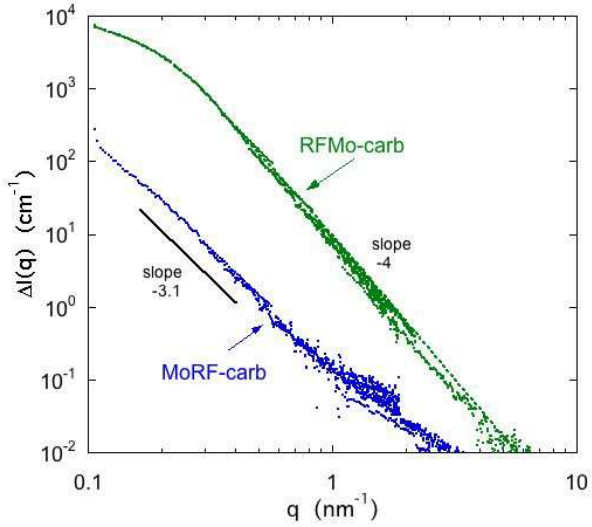

Figure 5. $\Delta I(q)$ in MoRF carb and RFMo-carb.

The behaviour of the difference signal $\Delta I(q)$ in the carbonised sample MoRF-carb is very different from that of RFMo-carb (Figure 5). While the elementary beads in MoRF-carb have

the power law slope -4 that is characteristic of smooth surfaces, in MoRF-carb the slope is approximately -3.1, indicative of scattering from extremely rough surfaces (surface fractal dimension 2.9). The intensity of MoRF-carb is also more than an order of magnitude smaller than that of RFMo-carb, in confirmation of its much lower Mo content. Nevertheless, the ratio of the anomalous intensity to the total signal in this sample, $\Delta I(q)/I_{19.8\mathrm{keV}}(q) = 0.117$, remains large, and implies that the Mo, owing to its high electron density, still dominates the scattering intensity. Since, however, the SAXS intensity is determined not only by differences in the electron density but also by the size of the scattering particles, these observations are insufficient to determine the molybdenum concentration of the samples.

3.2 Chemical state of molybdenum

According to TEM images the distribution of the molybdenum is strikingly different in the two carbon aerogels (Figure 6). 90 % of the Mo-particles are in the 25-60 nm and 8-20 nm range in the MoRF-carb and RFMo-carb samples, respectively. Surprisingly, the wet impregnation method results in a smaller particle size and a better dispersion of the metal.

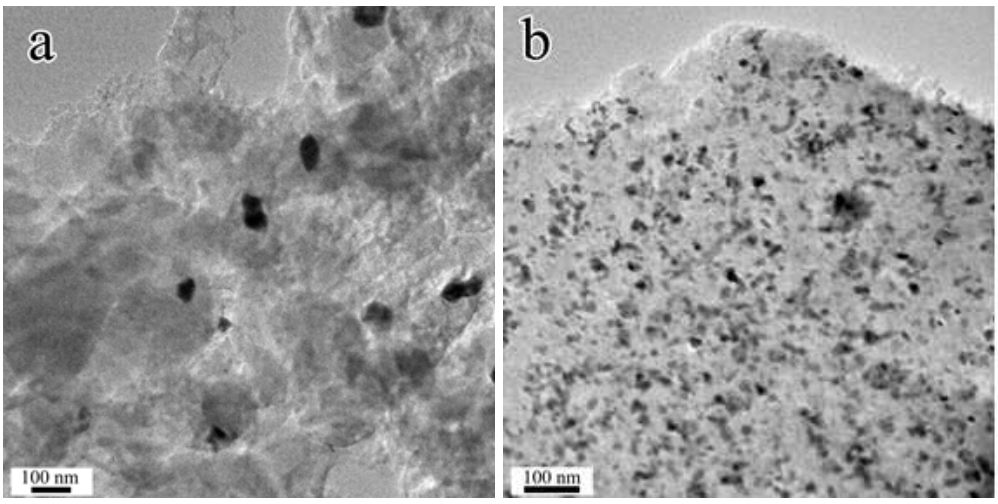

Figure 6 TEM images of MoRF-carb (a) and RFMo-carb (b) samples representing the distribution of Mo

The surface composition of the MoRF-carb and RFMo-carb samples, as well as the chemical states of the atoms on their surface were determined by XPS. The Mo 3d peaks can be resolved into three doublets (Figure 7). The less oxidised state of molybdenum appears only on the surface of the RFMo-carb sample. Its Mo $3d_{5/2}$ peak was found at binding energy 228.4 eV. This is almost 1 eV higher than the binding energy of both the metallic molybdenum and the molybdenum carbide. Since no other elements but carbon, oxygen and molybdenum were detected on the surface, and organic compounds would not survive the temperatures to which the sample was subjected, the peak must belong to a type of molybdenum oxide. It must be noted, however, that according to reference works both MoO_3 and MoO_2 appear at higher binding energies [36]. The peak therefore belongs to a suboxide of molybdenum that cannot be precisely identified due to lack of literature data on the XPS peak positions of such compounds.

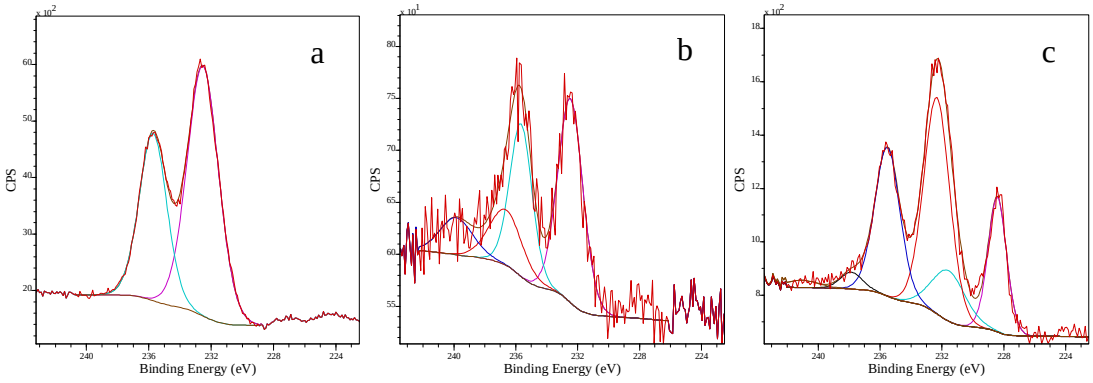

Figure 7 Deconvolution of the Mo $3d_{5/2}$ response in the XPS spectra.

Initial AM (a), MoRF-carb (b), RFMo-carb (c).

The Mo $3d_{5/2}$ peak of the more oxidised state appears at binding energy 232.4 eV in both samples. This matches the position of both the native oxide of molybdenum and the ammonium heptamolybdate used to dope the samples with molybdenum. Due to the thermal behaviour of ammonium heptamolybdate this second, more oxidised state probably belongs to MoO_3 [41]. (It must be noted however that pure, perfectly stoichiometric MoO_3 gives rise to

peaks at a slightly higher binding energy than native molybdenum oxide, or the compound detected on the surface of these samples. This means, that even this second state is slightly less oxidised than true MoO_3.) Besides these states, a third doublet peak was detected on both samples. The Mo $3d_{5/2}$ peak of these doublets appeared at 236.7 and 237.8 eV, respectively. Since no molybdenum compound exhibits such high chemical shifts, this third component must be the result of localised charging: both samples contain a small amount of insulating particles that are charged to a relatively high positive potential. Since this potential is unknown, the chemical state of molybdenum in these particles cannot be established. The concentration of molybdenum in this state is below 0.1 at% on the surface of both samples.

Table 3 Elemental composition (at%) of the doped carbon aerogels

Sample	**carbon**	**oxygen**	**molybdenum**			
			all	reduced	oxidized	from EDX
	C1s	O1s	Mo $3d_{5/2}$			
MoRF-carb	80.8	19.0	0.1	-*	0.1	0.29±0.04
RFMo-carb	82.0	16.5	1.5	0.4	1.1	2.24±1.28

* below the detection limit

The molybdenum content from EDX and XPS responses is compared in Table 3. The difference between the EDX and XPS data stems from the fact that EDX and XPS measures the bulk (several μm in our case) and the surface composition, respectively. The low Mo content of the MoRF-carb sample, also confirmed by the WAXS and XRD analyses, is due to poor retention of the Mo during the solvent exchange (the colour of the washing acetone turned blue) and shows that the Mo is not chemically bound [38].

XRD and SAED analyses were performed to determine the chemical form of the molybdenum in the bulk. No crystalline phase was found in the polymer aerogels. In MoRF-carb a very limited amount of crystalline α-Mo_2C phase was detected by XRD (Figure 8). In RFMo-carb the crystallinity is more pronounced and, as also revealed by wide angle X-ray scattering (WAXS) responses [42], an additional wide molybdenum carbide peak appears, reflecting the microcrystalline character of this phase (Figure 8). Figure 9 shows a HRTEM image of the MoRF-carb sample including both amorphous and crystalline areas. The insets represent a magnified section of an embedded crystal (upper right) and the corresponding FFT pattern (lower right). At the given imaging conditions, the FFT can be indexed on the basis of either η-Mo_3C_2 or α-Mo_2C phases as marked in Roman and italic characters, respectively.

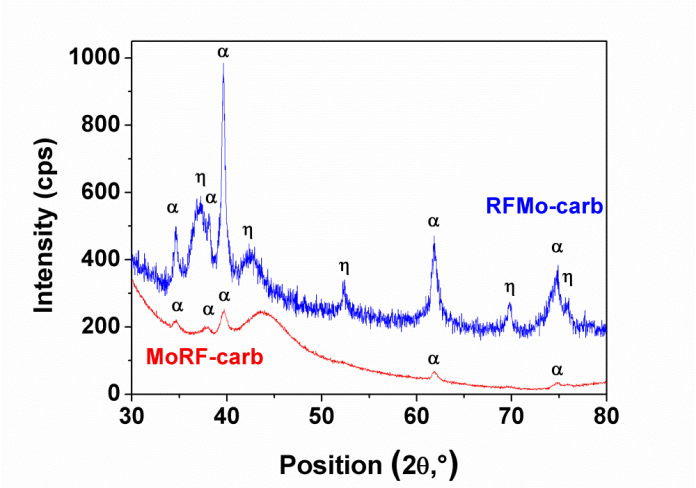

Figure 8 XRD patterns of the molybdenum doped carbon aerogels.

α and η denote peaks assigned to α-Mo_2C and η-Mo_3C_2, respectively. The weak intensity of the α peaks compared to that of the amorphous peak from the carbon substrate at 2θ≈44º (q=30 nm^{-1}) confirms the low Mo content of MoRF-carb.

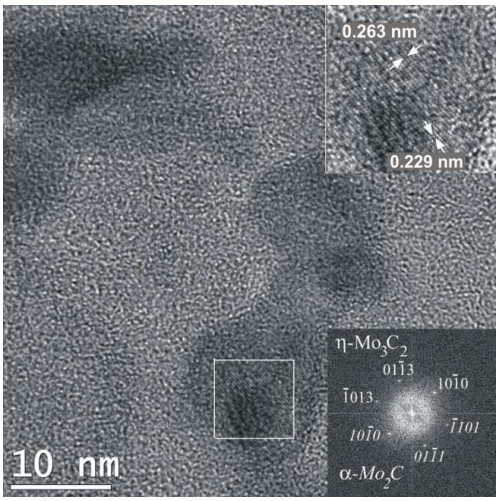

Figure 9 HRTEM image of the sample RFMo-carb. The upper right inset is the magnification of a crystalline area marked by a rectangle. The lower right inset is the corresponding FFT pattern that can be indexed as η-Mo_3C_2 and α-Mo_2C phases, indicated with Roman and italic characters, respectively.

It can be concluded that the chemical form of molybdenum is significantly different on the surface (oxides) and in the bulk (carbides). In molybdenum doped micro- and macroporous carbon aerogels surface and bulk carbides were detected only after post-treatment in H_2/Ar at 800 °C [43]. However, formation of molybdenum carbide was reported when a commercial micro- and mesoporous activated carbon was treated at 1000 °C in Ar or He [44]. The water that forms during the heat treatment may react with the carbon surface or with the CO from the degradation products:

$$H_2O+C = H_2 + CO \qquad (5)$$

and/or

$$CO + H_2O = H_2+CO_2 \qquad (6)$$

Both reactions lead to the *in situ* formation of H_2. In the narrow pores where the gas transport is limited and the residence time of the H_2 is long it may act as a reducing agent, resulting in

the formation of carbides in the bulk. On the open surface, however, the hydrogen is easily eliminated by the inert gas stream, thus preventing the formation of carbide.

3.3 Catalytic test reaction

The catalytic performance of Mo-doped carbon aerogels has already been reported in the isomerization of 1-butene and the aromatization of alkanes [18, 31]. In our experiments the molybdenum doped carbon gels were tested in the catalytic hydroconversion of AA. Three well separable pathways can be distinguished in this reaction: (I) hydrogenolysis, yielding carbon monoxide and methane; (II) ketonization producing carbon dioxide and acetone; (III) reduction of acetic acid, which may result in acetaldehyde, ethanol and ethyl acetate [37]. The change in the distribution of the compounds with time on stream is represented in Figure 10. In these *stacked area graphs* the concentration of a particular product is represented by the distance between two neighbouring lines [37]. Thus, the uppermost curve also shows the total conversion of the AA. Although the reaction conditions were not optimized, the comparison of these graphs clearly demonstrates enhanced catalytic activity with both Mo-doped samples. The overall concentration of acetaldehyde, ethanol and ethyl acetate after 6 hrs can be used to evaluate the performance of the three aerogels.

The low conversion rate (<15 %) and the distribution of the products are practically constant in time when the Mo-free carbon gel is used as catalyst. Nevertheless, the high yield of the gaseous products shows that route I is the determining pathway. The three liquids from route III amount to less than 21 %. The molybdenum doping significantly increases the catalytic activity. Although the conversion decreases slightly as the reaction progresses, it is much higher than without molybdenum, even after 6 hrs in both systems. The amount of gaseous products (e.g., carbon monoxide and methane) is very low. The best results are obtained over the RFMo-carb sample. Not only is the conversion highest but the distribution of the products

is the most favourable. No carbon monoxide or methane (typical of route I) were detected. The concentration of the high value solvents is 66 %, compared to the 52 % with the MoRF-carb sample. This improved performance can be partly explained by the higher molybdenum content of this carbon aerogel and the finer distribution of the metal, but the improvement is clearly not proportional to the molybdenum content. The distribution of the products clearly shows that the mechanism is influenced by the molybdenum present. Also, the time dependence of the product distribution reveals that the surface properties, particularly of the Mo-containing catalysts, undergo changes during the hydroconversion reactions.

A systematic investigation of the AA hydrogenation process with post-impregnated Mo-doped carbon aerogels including the influence of the Mo content on the reaction mechanism is reported elsewhere [45].

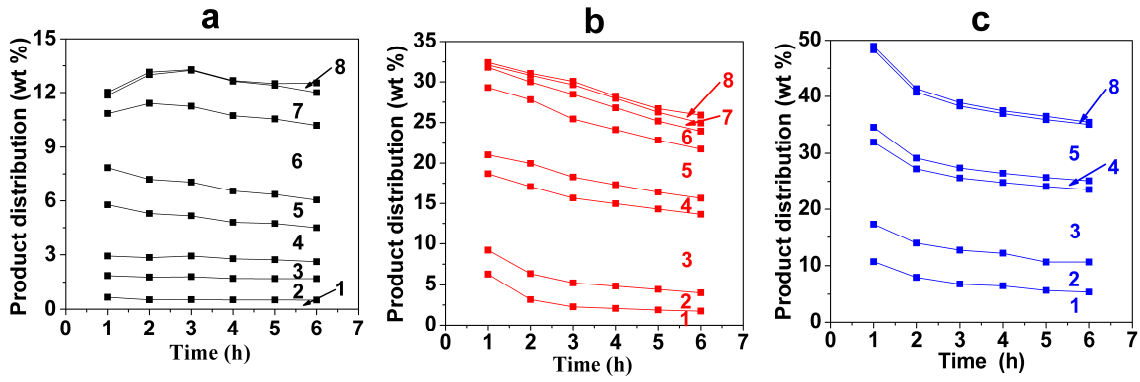

Figure 10 Evolution of the product distribution with the time on stream of the RF-carb (a), MoRF-carb (b) and RFMo-carb (c). The uppermost curve gives the total conversion of the AA. The concentration of a particular product is represented by the distance between two neighbouring lines. 1: ethanol, 2: acetaldehyde, 3: ethyl acetate, 4: acetone, 5: water, 6: carbon monoxide, 7: methane and 8: other products.

4. Conclusions

Molybdenum doped carbon aerogels were prepared by two different synthesis routes. Molybdenum was added either to the initial mixture or to the supercritically dried polymer matrix by the IWI method. It was found that both the morphology of the Mo doped RF matrices and the chemical state of Mo depend strongly on the synthesis route. The presence of molybdenum during the polymerization stage (MoRF) resulted in the development of much larger elementary spheres and a reduced porosity and surface area. The IWI treatment, in addition to suppressing the microporosity in the polymer aerogel, led to the formation of mesopores of width 3-15 nm. The carbonisation post-treatment substantially enhanced the surface area and the microporous character but the PSD in the mesopore range was conserved. Carbon aerogels with significantly different Mo-content and distribution were obtained. The IWI method gave a smaller particle size and a better dispersion of the metal. The Mo(VI) of the impregnating salt reduced to molybdenum carbide(s). In the bulk of RFMo-carb crystalline forms of α-Mo_2C and η-Mo_3C_2 were identified, while in the low Mo content MoRF-carb sample only a limited amount of α-Mo_2C was detected.

The presence of molybdenum improved the catalytic activity of the carbon aerogel in the hydrogenation reaction of acetic acid, a model compound for biomass, although the increase is not proportional to the metal content. The highest conversion and most valuable product distribution were obtained with the RFMo-carb sample. The relative enhancement in MoRF-carb compared to the Mo-free sample is, however, more dramatic given its low metal content. The combination of the more advantageous pore structure, the fine Mo-distribution and the probably more suitable chemical form altogether may also be responsible for the better performance of the RFMo-carb sample.

Acknowledgements

The support of the TÁMOP-4.2.2.A-11/1/KONV-2012-0043 (ENVIKUT) is gratefully acknowledged. The authors are grateful to the European Synchrotron Radiation Facility for access to the French CRG beam line BM2 and thank G. Bosznai for his contribution to the experiments.

References

[1] Hrubesh LW. Aerogel applications. Journal of Non-Crystalline Solids 1998; 225(1-3):335–342.

[2] Frackowiak E, Béguin F. Carbon materials for the electrochemical storage of energy in capacitors. Carbon 2001; 39(6):937–950.

[3] Babić B, Kaluđerović B, Vračar L, Krstaji N. Characterization of carbon cryogel synthesized by sol-gel polycondensation and freeze-drying. Carbon 2004 42(12-13):2617–2624.

[4] Zhu Y, Hu H, Li W, Zhang X. Resorcinol-formaldehyde based porous carbon as an electrode material for supercapacitors Carbon 2007; 45(1):160–165.

[5] Yuan X, Chao YJ, Ma ZF, Deng X. Preparation and characterization of carbon xerogel (CX) and CX-SiO composite as anode material for lithium-ion battery Electrochemistry Communications 2007; 9(10). 2591–2595.

[6] Smirnova A, Wender T, Goberman D, Hu YL, Aindow M, Rhine WN, et al. Modification of carbon aerogel supports for PEMFC catalysts. International Journal of Hydrogen Energy 2009; 34:8992–8997.

[7] Kim PH, Kwon JD, Kim JS. The impregnated synthesis of polypyrrole into carbon aerogel and its applications to photovoltaic materials. Syntetic Metals 2004; 142(1-3):153–160.

[8] Yamamoto T, Endo A, Ohmori T, Nakaiwa M. Porous properties of carbon gel microspheres as adsorbents for gas separation. Carbon 2004; 42(8-9):1671–1676.

[9] Pekala RW. Organic aerogels from the polycondensation of resorcinol with formaldehyde. Journal of Maretials Science 1989; 24(9):3221-3227.

[10] Lin C, Ritter JA. Effect of synthesis pH on the structure of carbon xerogels. Carbon 1997; 35(9):1271-1278.

[11] El Khatat AM, Al-Muhtaseb SA. Advances in Tailoring Resorcinol-Formaldehyde Organic and Carbon Gels. Advanced Materials 2011; 23:2887–2903.

[12] Czakkel O, Marthi K, Geissler E, László K. Influence of drying on the morphology of resorcinol–formaldehyde based carbon gels. Microporous Mesoporous Materials 2005; 86(1-3)124-133.

[13] Maldonado-Hódar FJ, Moreno-Castilla C, Pérez-Cadenas AF. Catalytic combustion of toluene on platinum-containing monolithic carbon aerogels. Applied Catalysis B-Environmental 2004; 54(4):217-224.

[14] Sánchez-Polo M, Rivera-Utrilla J, Méndez-Díaz J, López-Peñalver J. Metal-Doped Carbon Aerogels. New Materials for Water Treatments. Indrustrial & Engineering Chemistry Research 2008; 47(16): 6001−6005.

[15] Czakkel O, Szilágyi IM, Geissler E, László K. TiO2-doped resorcinol–formaldehyde (RF) polymer and carbon gels with photocatalytic activity. Nanomaterials and the Environment DOI: 10.2478/nanome-2013-0001.

[16] Czakkel O, Geissler E, Szilágyi IM, t Székely E, László K. Cu-doped resorcinol–formaldehyde (RF) polymer and carbon aerogels Journal of Colloid and Interface Science 2009; 337(2):513–522.

[17] Maldonado-Hódar FJ, Moreno-Castilla C, Rivera-Utrilla J, Hanzawa Y, Yamada Y. Catalytic graphitization of carbon aerogels by transition metals. Langmuir 2000; 16(9):4367-4373.

[18] Moreno-Castilla C, Maldonado-Hódar FJ, Rivera-Utrilla H, Rodríguez-Castellón E. Group 6 metal oxide-carbon aerogels. Their synthesis, characterization and catalytic activity in the skeletal isomerization of 1-butene. Applied Catalysis A: General 1999; 183(2):345-356.

[19] Maldonado-Hódar FJ, Jirglová H, Pérez-Cadenas AF, Morales-Torres S., Chemical control of the characteristics of Mo-doped carbon xerogels by surfactant-mediated synthesis. Carbon 2013; 51:213-223.

[20] Baumann TF, Fox GA, Satcher JH, Yoshizawa N, Fu R, Dresselhaus MS. Synthesis and Characterization of Copper-Doped Carbon Aerogels Langmuir 2002; 18(18):7073-7076.

[21] Cotet LC, Baia M, Baia L, Popescu IC, Cosoveanu V, Indrea E, et al. Structural properties of some transition metal highly doped carbon aerogels. Journal of Alloys and Compounds 2007; 434(SI):854–857.

[22] Carrott PJM, Marques LM, Ribeiro MML. Characterisation of the porosity of polymer and carbon aerogels containing Fe, Ni or Cu prepared from 2,4-dihydroxybenzoic acid by n-nonane pre-adsorption and density functional theory. Microporous and Mesoporous Materials 2010; 131(1-3):75–81.

[23] Fu R, Baumann TF, Cronin S, Dresselhaus G, Dresselhaus MS, Satcher JH Jr. Formation of graphitic structures in cobalt- and nickel-doped carbon aerogels. Langmuir 2005; 21(7):2647-2651.

[24] Saquing CD, Kang D, Aindow M, Erkey C. Investigation of the supercritical deposition of platinum nanoparticles into carbon aerogels. Microporous and Mesoporous Materials 2005; 80(1-3):11–23.

[25] Park HW, Hong UG, Lee YJ, Song IK. Catalytic decomposition of 4-phenoxyphenol to aromatics over palladium catalysts supported on activated carbon aerogel bearing sulfonic acid group. Catalysis Communications 2012; 20:89–93.

[26] Miller JM, Dunn B. Morphology and electrochemistry of ruthenium/carbon aerogel nanostructures. Langmuir 1999; 15(3):799-806.

[27] Lee YJ, Jung JC, Park S, Seo JG, Baeck SH, Yoon JR. Preparation and characterization of metal-doped carbon aerogel for supercapacitor. Current Applied Physics 2010; 10(3):947–951.

[28] Bozbag SE, Zhang LC, Aindow M, Erkey C. Carbon aerogel supported nickel nanoparticles and nanorods using supercritical deposition. Special Issue. Journal of Supercritical Fluids 2012; 66:265– 273.

[29] Fu R, Dresselhaus MS, Dresselhaus G, Zheng B, Liu J, Joe Satcher Jr, et al. The growth of carbon nanostructures on cobalt-doped carbon aerogels. Journal of non-crystalline solids 2003; 318(3):223-232

[30] Moreno-Castilla C, Maldonado-Hódar FJ. Carbon aerogels for catalysis applications: An overview. Carbon 2005; 43(3):455-465.

[31] Maldonado-Hódar FJ. Metal-doped carbon aerogels as catalysts for the aromatization of n-hexane. Applied Catalysis A: General 2011; 408(1-2):156-162.

[32] Czakkel O, Székely E, Kocka B, Geissler E, László K. Drying of resorcinol-formaldehyde gels with CO2 medium. Microporous and Mesoporous Materials 2012; 148(1):34-42.

[33] Brunauer S, Emmett P, Teller E. Adsorption of gases in multimolecular layers. Journal of American Chemical Society 1938; 60:309-319.

[34] Dubinin MM, Radushkevich LV. The equation of the characteristic curve of the activated charcoal, Proc. Acad. Sci. USSR Phys. Chem. Sect. 1947; 55: 331–337.

[35] Gor YG, Thommes M, Cychosz KA, Neimark AV. Quenched solid density functional theory method for characterization of mesoporous carbons by nitrogen adsorption. Carbon 2012; 50(4):1583-1590.

[36] Wagner CD, Riggs WM, Davies LE, Moulder JF, Muilenberg GE. Handbook of X-ray Photoelectron Spectroscopy. Perkin-Elmer, Eden Prairie 1979.

[37] Onyestyák Gy, Harnos Sz, Kaszonyi A, Štolcová M, Kalló D. Acetic acid hydroconversion to ethanol over novel InNi/Al2O3 catalysts. Catalysis Communications 2012; 27:159-63.

[38] Nagy B, Czakkel O, László K. New synthesis route of molybdenum doped resorcinol-formaldehyde polymer xerogels with tuned porosity. Submitted to Microporous and Mesoporous Materials.

[39] Debye P, Bueche AM. Scattering by an inhomogeneous solid. J. Appl. Phys. 1949; 20:519-525.

[40] http://skuld.bmsc.washington.edu/scatter/AS_periodic.html (29/07/2013)

[41] Hanafi ZM, Khilla MA, Askar MH. The thermal decomposition of ammonium heptamolybdate. Thermochimica Acta 1981; 45:221-232.

[42] Nagy B, Madarász J, Geissler E, László K. Molybdenum-containing RF and carbon aerogels. Extended abstract, International Carbon Conference 2011, Shanghai, China; CD-ROM of Extended Abstracts

[43] Pérez-Cadenas AF, Maldonado-Hódar FJ, Moreno-Castilla C. Molybdenum carbide formation in molybdenum-doped organic and carbon aerogels. Langmuir 2005, 21:10850-10855

[44] Mordenti D, Brodzki D, Djéga-Mariadassou G. New Synthesis of Mo_2C 14 nm in Average Size Supported on a High Specific Surface Area Carbon Material. J. Solid State Chemistry 141, 114-120 (1998).

[45] Ábrahám D, Dobos G, Madarász J, Onyestyák Gy, László K. Hydroconversion of acetic acid by carbon aerogel supported molybdenum carbide catalyst. Submitted to Journal of Catalysis